Growth and magnetic properties of Fe films on InP(001)

Florin Zavaliche, Wulf Wulfhekel, and Jürgen Kirschner
Max-Planck-Institut für Mikrostrukturphysik, Weinberg 2, D-06120 Halle, Germany
(Received 25 September 2001; revised manuscript received 28 January 2002; published 18 June 2002)

An investigation of the InP(001) surface and the characterization of thin Fe films grown on this substrate at ≈150 and ≈300 K are presented. As substrates, highly ordered P-rich (2×4) reconstructed surfaces obtained by Ar^+ ion bombardment at ≈570 K were used. The growth of Fe films in the submonolayer thickness range and the magnetic properties of thin Fe films grown on P-rich (2×4) InP(001) are reported. We observe a uniaxial in-plane magnetic anisotropy up to an Fe thickness of ≈14 monolayers, which is related to the uniaxial character of the InP(001) reconstruction. From the magnetization behavior we obtained the surface/interface contribution to the uniaxial anisotropy, and deduced that very small, if any, magnetically dead layers form at the interface. Auger electron spectroscopy data reveal that about one monolayer of In segregates to the top of the growing Fe film at ≈300 K, but does not support a strong Fe-InP(001) intermixing, in contrast to the current belief. The current-voltage characterization of patterned Fe films grown on *n*-InP(001) shows nonrectifying contacts at room temperature.

DOI: 10.1103/PhysRevB.65.245317 PACS number(s): 68.35.−p, 75.70.Ak, 68.55.−a

I. INTRODUCTION

A strong interest towards the investigation of the ferromagnet-semiconductor interface has been triggered by the work of S. Datta and B. Dass[1] who proposed a spin-electronic analog of the electro-optic light modulator, opening thus the way to what was later called magnetoelectronics.[2] In spite of the large amount of experimental effort focused on the topic, a recent work imposed severe restrictions on the functionality of integrated ferromagnetic metal-semiconductor solid-state devices.[3] Instead, it was proven that an entirely semiconductor-based system is feasible,[4] however, only under extreme conditions of low temperatures and high magnetic fields.

From the pragmatic requirement of functionality with small magnetic fields and at environmental temperatures, the concept of spin injection into semiconductors needs substantial modifications, e.g., by the integration of a tunnel junction to produce hot electrons as part of the spintronic device.[5] Alternatively, spin polarized electrons can be generated in a metal-based spin-valve structure in which hot electrons are injected and then filtered by the Schottky barrier.[6] Therefore the presence of a uniform Schottky barrier appears to be crucial for the feasibility of the device.[7] If a tunnel junction is used as the source of hot spin-polarized electrons, the presence of an additional barrier at the metal-semiconductor contact might not necessarily be beneficial. To maintain a high spin polarization of hot electrons passing into the semiconductor, where the signal is actually processed, it is necessary that the electrons see a reduced amount of interface states. These interface states, which may trap the tunneling electrons on their way to the bulk semiconductor, are responsible for the Fermi-level pinning and give rise to an enhancement of the Schottky barrier.[8] Therefore, even if hot electrons are to be used for spin injection into semiconductors, it appears that low rectifying contacts are highly desired. In addition, a nonmagnetic layer at the interface between the ferromagnet and the semiconductor, usually structurally disordered, might act on the traveling hot electrons as strong spin scatterers, preventing thus the spin information being transferred into the semiconductor; all these facts should be considered in the choice of the proper ferromagnet-semiconductor system.

Among the possible candidates for substrates we selected the InP(001) for interesting physics is expected to emerge upon the growth of thin Fe films on a semiconducting substrate which shows a lattice mismatch $(a_{InP(001)}-2a_{Fe})/2a_{Fe}$ of only +2.2%. In addition, the InP(001) surface shows, under certain conditions, a (2×4) reconstruction which does not resemble any one seen on other III-V compound semiconductors.[9,10] Also, the relevance of InP(001) in the field of high-speed (opto-)electronics and the possibility of realizing low rectifying contacts[11,12] were kept in mind. However, strong reactions were previously shown to occur at the interface, leading to the formation of metallic phosphide compounds and to In out-diffusion.[12–15] In this context, it has been also reported that metal films which strongly react with the semiconductor anion give rise to small Schottky barrier heights.[14,15] The attempt of growing P- and In-free Fe films on S-passivated InP(001) failed:[16] the S-terminated surface is disrupted upon Fe deposition, and, while the substrate InP(001) core-level photoemission signal has been completely attenuated, the P, In, and, in addition, the S chemically shifted components of the spectra are clearly visible even for ordered Fe films.

The surface of InP(001) prepared by sputtering at elevated temperatures was characterized with respect to its structure and morphology, prior to the deposition of Fe films. We show that a highly ordered surface is obtained in this way. In this work, thin Fe films of thickness ranging from the submonolayer coverage to almost 20 monolayers were grown by molecular-beam epitaxy on such substrates. The films were characterized with respect to their structural, morphological, compositional, and magnetic properties, and our findings do not support a strong film-substrate intermixing. We show in this work that thin Fe films grown on InP(001) show appealing properties which makes the system a candidate for being integrated into high-speed magneto-optic technology.

II. EXPERIMENT

Pieces of about $0.4\times2\times10$ mm^3 were cut from Wafer Technology Ltd. undoped *n*-InP(001) $\pm0.25°$ wafers with a specified electrical resistivity of 3.0×10^{-1} Ω cm, and mounted on molybdenum holders equipped with radiative heating facilities. No chemical treatment was carried out prior to inserting the sample into the ultrahigh vacuum (UHV) chamber via a load lock system. The substrates were first degassed in UHV up to about 570 K, and then sputtered for 30 min at the same temperature with a 500 eV Ar^+ ion beam at an incidence angle of 45°. The samples were rotated around their normal during sputtering to reduce the degree of surface roughening. At a partial Ar pressure of about 5×10^{-8} mbar, a sputtering current density of about 0.02 μA/mm^2 was measured. The compositional investigation of the surface was performed by Auger electron spectroscopy (AES), while the structural and morphological information were obtained by low-energy electron diffraction (LEED) and scanning tunneling microscopy (STM). The STM scans were performed at room temperature (RT) in the constant current mode. The Fe (99.99% purity) deposition was performed by means of an *e*-beam evaporator at growth rates of about 1.5 monolayers (ML's) per minute, where the monolayer coverage is defined in terms of the atomic density of bcc Fe(001), i.e., 1.22×10^{15} atoms/cm^2. The low-temperature (LT) growth was performed by cooling the sample holder with liquid nitrogen down to 150 K. The magnetization was probed by the magneto-optic Kerr effect (MOKE) in longitudinal geometry at an optical wavelength of 670 nm and an angle of incidence of $\approx50°$. The maximum dc magnetic field reachable with our setup was 30 mT. Henceforth it will be understood that film growth as well as substrate and film characterization were carried out *in situ* at a base pressure better than 7.0×10^{-11} mbar. For electrical characterization, a patterned Fe film of about 25 ML thickness capped with a protection layer of Au was grown at RT on an *n*-type InP(001) for *ex situ* current-voltage (I-V) characterization. The patterning into disks of $100-\mu$m diameter laterally separated by 50 μm was performed *in situ* by means of deposition through a shadow mask with the a mesh flipped over the cleaned substrate. Due to the low lateral dimension of the patches distributed over the sample, the measurements were performed in the two-point geometry.

III. RESULTS AND DISCUSSIONS

A. The (001) surface of InP

The (001) surface of InP has been investigated recently with respect to the types of reconstructions and terminations that can be assessed under different preparation conditions.[9,10,17–30] Different surface reconstructions after sample preparation were found, of which the most important are the In-rich (2×4) and $c(2\times8)$, and the P-rich (2×4) and $c(2\times8)$ phases. A high-resolution STM investigation of the In-rich (2×4) phase promoted a trimer model.[9] For P-rich (2×4) a mixed In-P dimer model was proposed.[10]

The ion bombardment and annealing (IBA) of InP(001) has been shown[31–34] to yield an In-rich $(4\times2)/c(8\times2)$ reconstruction. However, our cleaning procedure seems to yield a P-rich surface as we determined by AES [Fig. 1(a)], with a ratio between the peak-to-peak intensities of the P_{LMM} line at 120 eV and In_{MNN} line at 404 eV of 1.20 ±0.05. No traces of contaminants were seen in the AES spectra. Annealing beyond 600 K, that is, close to the decomposition temperature, In droplets start to form and a hazy appearance of the surface is noticed, while the sharp (2×4) LEED pattern persists. Our procedure always yields a droplet-free surface with large terraces, as can be seen in the STM scans [Fig. 1(b)], with predominantly bi-atomic step edges. The (2×4) reconstruction we observed in LEED [the inset of Fig. 1(b)] appears in the STM topographs as rows running along $[\bar{1}10]$ [Figs. 1(b) 2(a), and 2(b)). The row distances are consistent with the size of the (2×4) unit cell. High-resolution STM images, see Fig. 2(b), suggest a trimerlike reconstruction of the rows, possibly associated with the formation of mixed In-P dimers.[10]

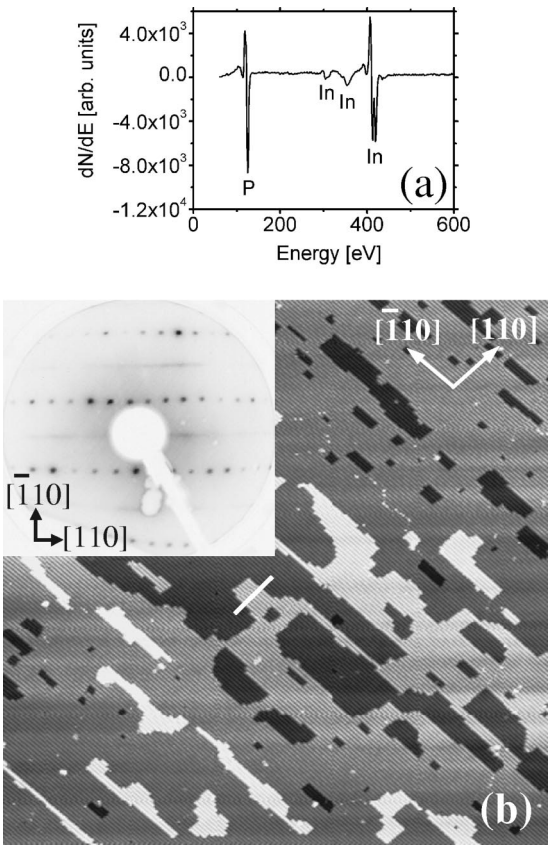

FIG. 1. The surface of InP(001) after sputtering and annealing: (a) the AES spectrum showing the P and In lines; (b) a 300 $\times300$ nm^2 STM scan performed at a bias voltage of -2.7 V and a constant tunneling current of 0.3 nA. Only four layers are visible at this scan range. The inset shows a (2×4) LEED pattern taken at a beam energy of 57 eV.

The LEED pattern displayed in the inset of Fig. 1(b) shows sharp (1×4) spots and intensity modulated streaks along [110] at the superstructure half order positions, indicative of a significant degree of disorder at first sight, in contrast to the highly ordered STM images. The apparent inconsistency with the high degree of order we observed in the

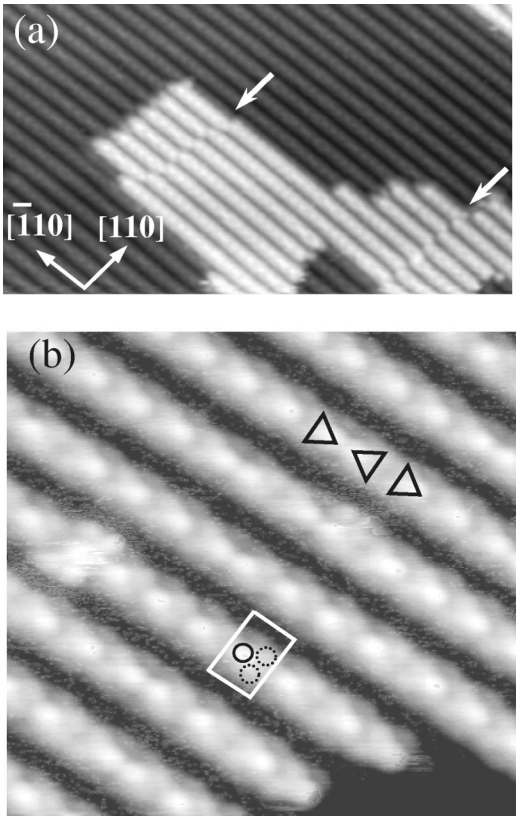

FIG. 2. High-resolution STM scans performed at the same tunneling parameters as in Fig. 1(b). (a) 50×30 nm^2: the row displacements are marked with white arrows; (b) 10×10 nm^2: the (2×4) unit cell comprising the mixed P-In dimers indicated with circles is shown. The solid circle marks the bright central dimer.

STM images might, at first sight, be simply explained by shifts of adjacent dimers in the [110] direction as also reported earlier.[9,35] These dimer displacements are accompanied by shifts in the same direction of entire groups of rows, without affecting the row position on the neighboring terraces. This kind of row displacements are pointed out by the white arrows in Fig. 2(a). If the reconstruction rows shift along [110] [Fig. 2(a)] by $5.87\times\sqrt{2}/2$ Å, i.e., by 4.15 Å, it was suggested that the quarter LEED spots remain unchanged, and only the half order ones become streaky.[9,35] However, the minimum lateral size of the shifted domains is of the order of 100 Å, which accounts for about 4% of the surface Brillouin zone (SBZ). In other words, this corresponds to a half order spot broadening along [110] with 4% of the distance between the (00) and (01) spots. Thus it is obvious that the mechanism described above will not result in any conspicuous departure from a sharp (2×4) pattern with very well defined half order spots. Accordingly, their complete wipe out must be induced by a mechanism which originates from the atomic scale disorder, as described in the following.

A careful inspection of the high-resolution filled states STM image in Fig. 2(b) reveals details on the ''packing'' of dimers. The observed trimerlike appearance of the unit cell was shown to be comprised of mixed In-P and missing dimers.[10] Accordingly, we associate the central brightest feature in the cells with a topmost In-P dimer. Two additional weaker features, P anions, are visible as protrusions in the STM filled state images, forming a trianglelike peculiarity with the mixed dimer in the first layer. The features were marked accordingly with circles in the (2×4) unit cell depicted in Fig. 2(b). By inspecting the sequences of the trimerlike features along the reconstruction rows [the triangles in Fig. 2(b)] we bring an evidence for disorder in the packing.[10] Therefore, as suggested by Guo *et al.*,[10] the disorder induced by these three distinct packings on the electron density stands for the real mechanism responsible for the occurrence of streaks in the LEED pattern.

B. Fe grown on InP(001)

In contrast to the abundance of work concerning the magnetic, structural and morphological properties of ferromagnetic films grown under different conditions on the most widely used semiconductors, i.e., Si(001) and GaAs(001), there are few data published on thin Fe films grown on the technologically relevant (001) surface of InP. So far, to the best of our knowledge, only the chemical reaction between thin Fe films and S-passivated InP(001) has been investigated,[16] and no information on the magnetic behavior has been reported up to date.

1. Growth investigation

In our experiments, thin Fe films were grown on (2×4) P-rich InP(001) at substrate temperatures of ≈150 (LT) and ≈300 K (RT). For the growth characterization, only the RT case was considered since the transport into the STM is performed via uncooled manipulators. The early growth stages are investigated in the thickness regime starting from fractions of a monolayer up to several ML's. The deposition of a minute amount of Fe, i.e., ≈0.2 ML, is able to almost completely wipe out the streaks at half order position in the LEED pattern [Fig. 3(a)], and a stronger background is noticed. It appears that an increased disorder is induced by the growing of small size Fe islands, but no preferred growth direction can be seen in the filled states STM image in Fig. 3(b). The regular and sharp appearance of the substrate reconstruction, like the one shown in the STM scan in Fig. 2(a), becomes smeared out by the Fe islands, but the overall rowlike characteristic is preserved. Thus it seems that the Fe islands prefer to nucleate atop the rows rather than in the troughs between them. The line scan in Fig. 3(c) taken along substrate [$\bar{1}$10] direction over one of the reconstruction rows gives us a hint about the island sizes. The observed ≈1.5 Å corrugation in Fig. 3(c) is assigned to the irregularly separated Fe islands, of 1 ML thickness. The most predominant island lateral size is ≈1 nm, which stands for approximately 7 ± 1 Fe atoms. These numbers point at the same island size as in the case of ≈0.2 ML of Fe grown on As-rich (2×4) GaAs(001).[36] The addition of slightly more Fe to a total thickness of 0.4 ML is not able to disrupt the reconstruction, since sharp LEED spots were still observed [Fig. 3(d)], and the rowlike appearance in the filled states STM image persists to some extent [Fig. 3(e)]. Therefore small Fe islands and (2×4) reconstructed areas coexist at least up to 0.4 ML.

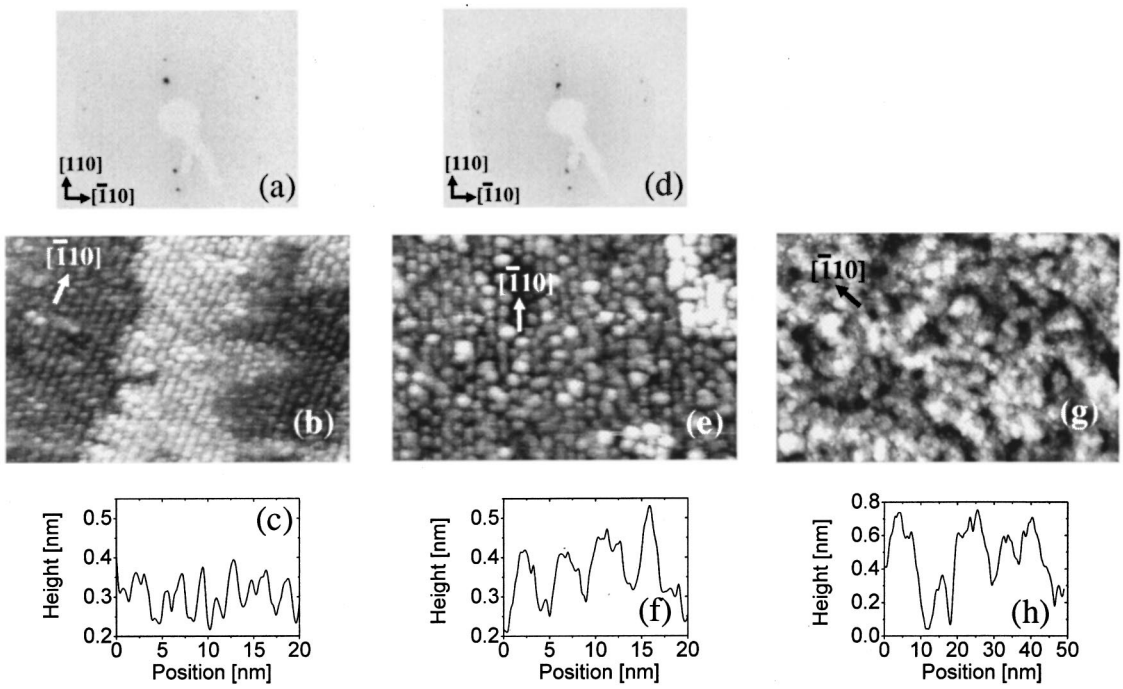

FIG. 3. LEED patterns taken at a beam voltage of 52 eV, and 75×50 nm^2 STM scans of RT grown Fe films of thickness $\lesssim 0.2$ ML, (a) and (b), and of ≈ 0.4 ML, (d) and (e). The STM images were taken at a bias voltage of -2.7 V and constant tunneling currents of 0.3 and 0.1 nA, respectively. The line scans shown in (c) and (f) were taken along the substrate's [$\bar{1}$10] direction. A 75×50 nm^2 STM scan of $\lesssim 4$ ML Fe grown at RT performed at 1.4 V bias voltage and 0.1 nA constant tunneling current, and a line profile are shown in (g) and (h), respectively. The substrate symmetry axes are marked on the figures.

The line scan in Fig. 3(f) taken along substrate [$\bar{1}$10] over one of the rows reveals larger Fe islands than in $\lesssim 0.2$ ML thick film, with the distribution of the lateral sizes around several nanometers. Most of the islands are 1 ML thick, but also 2 ML thick islands are observed. Such ''tall'' islands can be seen as brighter bumps in Fig. 3(e) and are generally associated with larger islands lying over two substrate rows. One can state that the growth of 3D islands proceeds very early at RT.

Starting with an Fe thickness of ≈ 1 ML no LEED pattern could be seen any longer up to the thicknesses investigated, and the rowlike appearance is completely obscured. Therefore a high degree of structural disorder in the film or on the surface of the growing film is inferred. This finding is in contrast to the reappearance of a sharp LEED pattern in the case of RT Fe growth in excess of about 3 ML on GaAs(001),[37] which cannot be solely explained by the differences in the sign and magnitude of the lattice misfits: $(a_{substrate}-2a_{Fe})/2a_{Fe}=+2.2\%$ and -1.6% for InP(001) and GaAs(001) substrates, respectively. The reason for the high disorder in the Fe film grown on InP(001) is not clear. At an Fe thickness slightly below 4 ML, the film is characterized by small three dimensional (3D) coalesced islands, and no preferred orientation can be distinguished [Fig. 3(g)]. The islands are irregular and their heights vary between 2 and 5 ML as can be deduced from the line profile in Fig. 3(h). Thus the RT deposition does not result in the growth of a smooth film.

2. Magnetic characterization

In contrast to the apparent disordered growth, magnetic measurements point at some order in the film, as described below. During LT and RT Fe growth, the magnetization behavior was probed *in situ* by the longitudinal magneto-optic Kerr effect (MOKE), for fields along the two relevant substrate symmetry directions, [$\bar{1}$10] and [110], that is, parallel and perpendicular to the reconstruction rows. Shortly after the ferromagnetic order sets in, the loops taken at LT [Figs. 4(a) and 4(b)] and RT [Fig. 4(c) and 4(d)], for 2.6 and 3.6 ML thick films, respectively, reveal a strong uniaxial in-plane magnetic anisotropy behavior similar to the case of Fe grown on GaAs(001):[38] while hysteresis open up in square-like shapes for fields along [$\bar{1}$10] [Figs. 4(b) and 4(d)], pure rotation loops were observed along [110] [Figs. 4(a) and 4(c)], regardless of the growth temperature. We can denote the substrate [$\bar{1}$10] direction as the easy axis of magnetization for the Fe film, and the [110] one as the hard axis. Thus the magnetic anisotropy of the film point at some order, in contrast to the LEED results. The magnetization appears to be fully rotated parallel to [110] at fields of roughly one order of magnitude higher than the coercive fields of the hysteresis measured along [$\bar{1}$10]. For the two growth temperatures and for the whole range of thickness investigated, the easy axis was found to lie in-plane, and no perpendicular component of magnetization was detected. The discrepancy between the lack of any LEED pattern and the order inferred by the uniaxial behavior of magnetization might be ex-

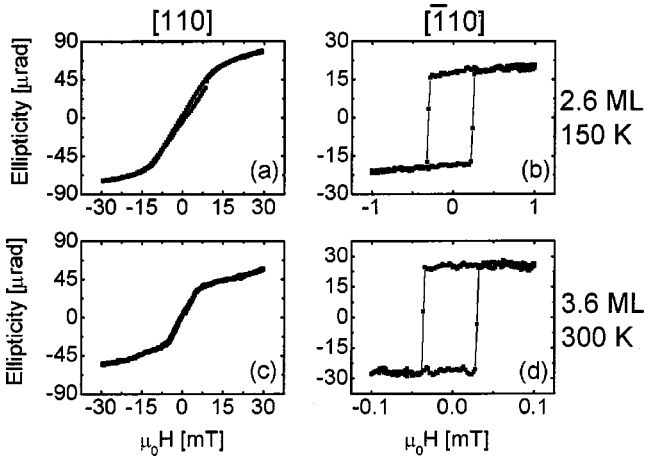

FIG. 4. In-plane magnetic loops taken shortly after the magnetization onset at both ≈150 and ≈300 K, i.e., for Fe film thicknesses of 2.6 and 3.6 ML respectively. The magnetic field was oriented along the two relevant crystallographic directions of the substrate: (a) [110] and (b) [$\bar{1}$10] at ≈150 K. The loops in (c) and (d) were measured at ≈300 K, for the same field orientations.

plained by assuming a high degree of disorder at the film's growth front induced by In segregation, as we will see in the forthcoming section. The uniaxial behavior of the in-plane magnetic anisotropy persists up to about 13–15 ML, and cannot be related to any shape anisotropy of the incipient growing film. Therefore the uniaxial character of the substrate's (2×4) unit cell, and implicitly of the interface may bear the whole responsibility for the magnetic anisotropy we found.

From the saturation field of the pure rotation loops measured along [110] [Figs. 4(a) and 4(c)] we estimated the magnitude of the in-plane uniaxial magnetic anisotropy constant[39] at the onset coverage: $K_u=I_sB_s/2\mu_0\approx1.2\times10^4$ J/m^3 for films grown at ≈150 K and $\approx0.8\times10^4$ J/m^3 in the RT growth case [see the lowest coverage data points in Fig. 5(a)]. In the above approach, I_s stands for the saturation magnetization of iron (2.16 T), and B_s $[T]$ for the magnetic flux density necessary to fully rotate the magnetization along [110]. For comparison, one can notice that the measured K_u values in both LT and RT growth cases are much lower than the magnetocrystalline fourfold magnetic anisotropy K_1 for bcc Fe at RT (4.72×10^4 J/m^3). The stronger anisotropy we found for films grown at LT suggests a sharper interface than in the RT case. In the first growth stages shortly after the ferromagnetic order sets in, an increase in the strength of the in-plane magnetic anisotropy constant can be seen [Fig. 5(a)] regardless of the growth temperature. The weakened anisotropy we found for the very thin films is due to the measurements being performed close to their Curie temperatures. As the films thickness are increased, their Curie temperature rises, and the measured anisotropies reach their maxima at ≈3.5 ML for films grown at LT and ≈5 ML in the RT growth case. Afterwards, a monotonous decrease of the anisotropy strength with increasing coverage can be observed.

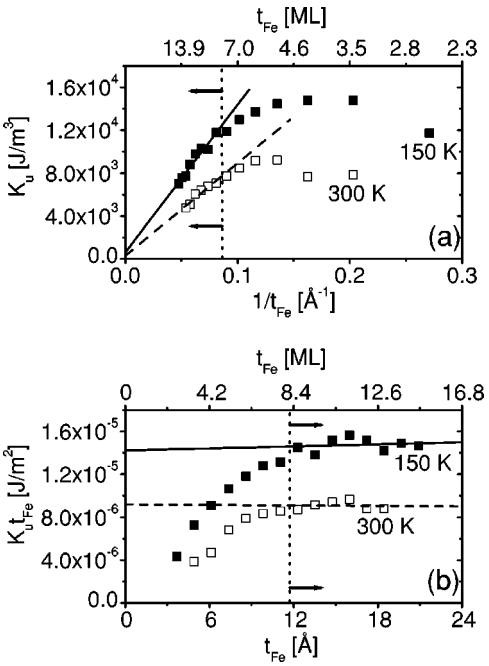

FIG. 5. The dependence of the in-plane magnetic anisotropy constant K_u with respect to inverse coverage $1/t_{Fe}$ (a), and the coverage dependence of K_u times the film thickness t_{Fe} (b). The solid and dashed lines stand for linear fits of the anisotropy data points above ≈8 ML in the case of ≈150 K (the solid squares) and ≈300 K (the open squares) growth temperatures.

If the anisotropy of a thin film, K_u, can be described by two anisotropy contributions, a volume contribution K_V in terms of energy per unit volume, and K_I defined in terms of energy per unit area, then the total anisotropy energy K_ut per unit area can be written as

$$K_ut=K_Vt+K_I. \tag{1}$$

Therefore we plot the measured K_ut_{Fe} values for the two growth temperatures as a function of thickness t_{Fe} in Fig. 5(a). These plots show an initial increase, then saturate at constant values. The constants mean that for large thicknesses the volume-dependent term becomes vanishingly small, as expected.

Alternatively, Eq. (1) may be rewritten as

$$K_u=K_V+\frac{1}{t_{Fe}}K_I. \tag{2}$$

This representation is rather popular, but can be misleading: if one plots K_u vs $1/t_{Fe}$, one often observes curves with two approximately linear slopes. Such behavior can be clearly seen here at both growth temperatures [Fig. 5(a)]. Therefore one needs a criterion to tell which slope should be considered for the extrapolation to $t_{Fe}\to\infty$ or $1/t_{Fe}\to0$. The intersection with the K_u axis for $1/t_{Fe}\to0$ yields, according to Eq. (2), the volume anisotropy, while the slope yields the interface contribution. The needed criterion is provided by the plots in Fig. 5(b), which show that for large thicknesses (i.e., $1/t_{Fe}\to0$) the volume anisotropy becomes very small or zero, as it should be, for there is no uniaxial volume contri-

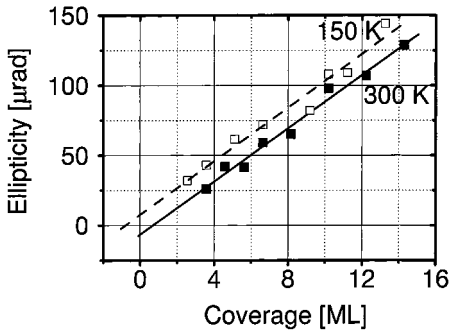

FIG. 6. MOKE remanence deduced from the loops measured along $[\bar{1}10]$ vs the Fe coverage at ≈ 150 and ≈ 300 K. Linear fits of the data points intersect the coverage axis at -0.5 ± 0.7 and $+0.8\pm0.4$ ML, respectively.

bution to the total magnetic anisotropy in unstrained bulk bcc Fe. Therefore the extrapolations must be done on the left-hand side of the plots in Fig. 5(a), yielding volume anisotropies K_V of $0.3\pm0.8\times10^3$ J/m^3 for films grown at 150 K and $0.0\pm0.9\times10^3$ J/m^3 for the 300 K growth case. The slopes yield the interface contributions K_I of $14.2\pm1.3\times10^{-6}$ J/m^2 at 150 K and $9.2\pm1.3\times10^{-6}$ J/m^2 at 300 K. These values are about two orders of magnitude smaller than the magnetocrystalline fourfold magnetic anisotropy K_1 for unstrained bcc Fe at RT (4.72×10^4 J/m^3). Films thinner than ≈ 8 ML appear to undergo modifications which prevent us from extending the analysis closer to the magnetization onset coverage. However, the important result is that, in contrast to the lack of any LEED pattern, the uniaxial behavior of magnetization infers some order in the growing film.

In the above analysis, a distinction between the contributions of the two film interfaces is hard to make. In addition, the separation of the K_u in a volume contribution and an interface one is, generally, questionable for a few ML thick films,[40] but also throughout the whole thickness of certain thicker films, as, for instance, in the case of Ni on Cu(001).[41] Another factor which may obscure the linear dependence is the departure of the actual magnetization saturation from the bulk value due to the different film structure and chemical environment in ultrathin films. These facts, together with the Curie temperature effect, should restrict the data interpretation to film thicknesses of several monolayers above the magnetization onset coverage.

In the following, we provide evidence to support the existence of a net magnetization in the very first layer of Fe being deposited. The remanent ellipticity measured along the easy axis gives a good estimate of the degree of magnetization, and, by plotting it vs Fe thickness, valuable information can be obtained about the state of magnetization in the first layers by simply determining the intercept between the linear fit of the remanent ellipticity data points and the coverage axis. This is shown in Fig. 6 for the two growth temperatures investigated and the following values for the intercepts were found: -0.5 ± 0.7 ML for Fe films grown at LT and 0.8 ± 0.4 ML in the RT case. The latter value would have been lower if the MOKE ellipticity had been measured farther from the Curie temperature of the film. Thus we can state

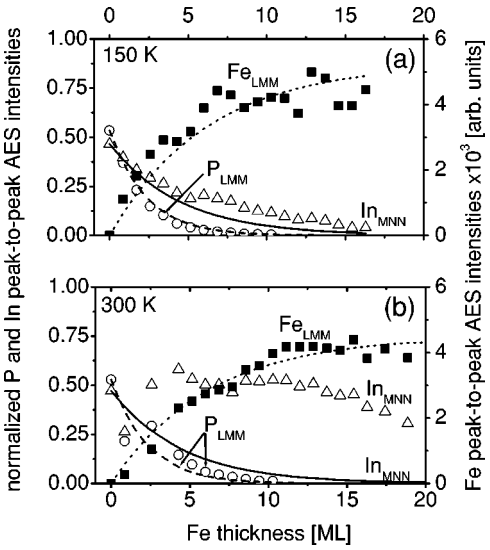

FIG. 7. AES peak-to-peak intensities of the Fe_{LMM} line at 651 eV (solid squares), along with the normalized AES peak-to-peak intensities of the P_{LMM} line at 120 eV (open circles) and In_{MNN} line at 404 eV (open triangles), measured for films grown at ≈ 150 K (a), and at ≈ 300 K (b). The dashed and solid curves stand for the predicted P and In normalized intensities, respectively, in the hypothesis of an ideal Fe growth (flat and continuous film as well as no intermixing). The dotted curves are fits of the Fe signal.

from this finding that the ferromagnetic order is likely present in the first layer of the growing film. No significant magnetically dead layers form at the interface between the substrate and the film, at least in the case of LT growth. The different numbers found above for the two growth temperatures infer different interfaces, in accordance with the different behavior of the uniaxial magnetic anisotropy we deduced in these two cases. The lack of a significant dead layer might be due to either a very sharp interface or to the formation of ferromagnetic Fe-based compounds, among which only ones with $\lesssim 27$ at. % P are known to possess a nonzero magnetization at RT.[42]

3. Compositional characterization

To judge the degree of intermixing, we performed an Auger electron spectroscopy (AES) investigation of the Fe films grown at both LT and RT. The evolution of the P_{LMM} line at 120 eV, the In_{MNN} one at 404 eV, and the Fe_{LMM} line at 651 eV were measured as a function of Fe film thickness. The normalized phosphorus and indium peak-to-peak intensities are shown in Figs. 7(a) and 7(b) for the two growth temperatures. The normalization of phosphorus and indium signals was done with respect to the sum of P_{LMM} and In_{MNN} peak-to-peak intensities at zero Fe coverage. Along with the experimental line intensities, the predicted P (the dashed line) and In (the solid curve) AES peak-to-peak intensities normalized as before are shown. The predicted curves were deduced by assuming an attenuation of exponential form according to

$$I^{P,In}=I_0^{P,In}\exp\left(-\frac{1.435t_{Fe}}{\cos\phi\lambda_{Fe}^{P,In}}\right) \tag{3}$$

with inelastic mean free paths (IMFP) in iron, λ_{Fe}^{P} and λ_{Fe}^{In}, of 4.6 Å for the 120 eV P_{LMM} Auger electrons,[43] and 8.6 Å for the 404 eV In_{MNN} ones.[43–45] Here, $I_0^{P,In}$ stands for the normalized substrate P_{LMM} and In_{MNN} intensities without attenuation, t_{Fe} is the Fe film thickness in ML's, and ϕ represents the admittance angle into the cylindrical mirror analyzer. In the above approach, we supposed that the deposited Fe forms a flat and continuous film, and no intermixing occurs at the interface. For both the sample and cylindrical mirror analyzer with electron gun had to be moved between the successive depositions/measurements, the scattering of the experimental data points appears quite strong, but valuable information can still be obtained.

From a first glance at the AES signals measured at the two growth temperatures, one can immediately see the different In line behavior from one case to the other: while the experimental signal follows rather closely the predicted curve of no intermixing at LT, an almost constant signal was observed at RT up to about 12 ML, followed by a rather slow decay. We associate this behavior with a substantial amount of In segregating to the top of Fe grown at RT, which gradually becomes buried into the growing Fe film as its thickness further increases, similarly to the finding of Hughes *et al.*[16] The almost constant In intensity measured at RT does not mean a constant amount of In floating on the top of the Fe film. If this were the case, the exponential decaying bulk contribution to the total measured signal would inflict a similar exponential behavior to the total signal throughout the thickness range investigated. Therefore, with increasing film thickness, an increasing amount of In segregates on the top of it, at least up to about 12 ML of deposited Fe.

The average amount of In segregating to the top of the Fe film at RT can be estimated by comparing the Fe_{LMM} signals measured at the two growth temperatures, and assuming that the reduced intensity measured at RT is solely due to absorption in the In overlayer. In the hypothesis of a negligible amount of In segregated at LT, and assuming an attenuation of exponential form, the evolution of the peak-to-peak iron intensities at LT and RT, can be fitted [the dotted curves in Figs. 7(a) and 7(b)]. The AES signal given by one Fe monolayer is deduced from the LT fit, and is assumed to be the same at both growth temperatures. Therefore, from the RT fit, the average thickness of the In segregated layer is estimated to be 2.0 ± 0.7 Å, which stands for about 1 ML (the lattice constant of tetragonal In is 4.59 Å).

Let us return now to the issue of the in-plane magnetic anisotropy. The two different growth temperatures give rise to the growth of Fe films whose interfaces are significantly different. While vacuum (and possibly some In)/Fe/P-rich InP(001) interfaces are encountered in the LT grown films, In/Fe/P-rich InP(001) interfaces are obtained in the RT case. The presence of segregated In and possibly an increased amount of P present at the RT grown film/substrate interface might lead to a disordered interface which potentially reduces the strength of the magnetic anisotropy. In contrast to the vanishing of the LEED pattern regardless of the deposition temperature, this fact points at the role of the uniaxial reconstruction of the substrate's surface. It seems that the uniaxial order at the interface is kept, which causes the uniaxial surface/interface anisotropy. In the RT case, the intermixing/segregation is stronger, probably due to a larger scale disruption of the substrate's dimers by the Fe adatoms. Thus the uniaxial character of the interface is accordingly reduced.

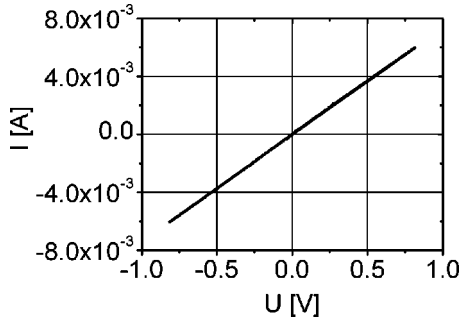

FIG. 8. The current-voltage characteristic performed at RT on a patterned 25 ML thick Fe film grown at ≈300 K on *n*-type InP(001); the separation distance between the patches (diameter of 100 μm) was about 100 μm.

By a careful comparison between the evolution of the experimental P_{LMM} AES intensity with the thickness of the LT grown film and its prediction curve [the open circles and the dashed line, respectively, in Fig. 7(a)], we can assert on the remarkably good agreement between each other. The exponentially decaying P_{LMM} intensity close to its prediction curve and its vanishing at about 11 ML of deposited Fe do not support the picture of a *strong* Fe-InP(001) intermixing with a significant Fe phosphide formation. Since vanishing magnetically dead layers were found at the interface, at most a minute amount of the ferromagnetically ordered compound whose stoichiometry is close to Fe_3P might form at the interface.

4. Electrical characterization

The other aspect mentioned in the introductory section, the height of the Schottky barrier, was also addressed in our study for the role it plays in processes associated with spin injection into semiconductors. For its estimate, we plot in Fig. 8 the current-voltage characteristic we measured *ex situ* on a patterned 25 ML thick Fe film grown at RT on *n*-type InP(001) and capped afterwards with Au to prevent the film oxidation. The measurement was performed in the two point geometry between two disk-shaped patches with diameters of about 100 μm, separated by approximately 100 μm. From the linear shape of the I-V characteristic we can state that no measurable Schottky barrier can be detected at RT. However, we are not able to asses the impact of the nonrectifying character of the Fe/*n*-InP(001) contact on the possible embedding of the system into the emerging spintronics.

IV. SUMMARY AND CONCLUSIONS

The surface reconstruction of Ar^+ ion sputtered InP(001) and the growth and magnetic behavior of thin Fe films grown on it at ≈150 and ≈300 K were investigated. We identify the highly ordered surface reconstruction we observed as the

P-rich (2×4) phase whose microstructure is associated with the existence of a mixed In-P dimer on the topmost layer. The different packing configurations of the (2×4) units occurring as the result of different sequences of mixed In-P dimers are strongly supported by our experimental findings. The growth of ultrathin Fe films on P-rich (2×4) InP(001) proceeds as 2D islands up to about 0.4 ML, and no hints about any in-plane preferred growth direction was found. Thereafter, 3D islands start to grow, which subsequently coalesce as the amount of deposited Fe increases. The films show a good ferromagnetic order with a strong uniaxial in-plane magnetic anisotropy up to an Fe thickness of about 15 ML at ≈150 K and 13 ML at ≈300 K with the easy axis along $[\bar{1}10]$. The uniaxial character of the underlying (2×4) substrate reconstruction is found responsible for this behavior. A stronger surface/interface anisotropy was found at LT $(14.2\pm1.3\times10^{-6}$ J/m$^2)$ in comparison to the RT growth case $(9.2\pm1.3\times10^{-6}$ J/m$^2)$. While less than 1 ML is found magnetically dead in the case of RT growth, all of the LT grown layers are proven to be magnetically alive. In addition to the onset of a magnetic interface, the RT grown Fe film–*n*-type InP(001) system is characterized by a nonrectifying contact. Contrary to the currently accepted belief, our AES investigation does not point at a *strong* intermixing between the Fe film and InP(001) associated with a large scale formation of Fe phosphide.

Our experimental findings support the possible implementation of the system in an integrated solid-state spintronic device as mentioned in the introductory section. The presence of a nonmagnetic interface can strongly enhance the spin-flip scattering of the polarized electrons generated in the ferromagnetic layer and impinging into the semiconductor. A magnetic interface, highly desirable for a longer spin lifetime, is expected to be encountered in such layer. Moreover, spin polarized electrons can also be generated within this layer, or it can act as a spin filter by itself.

[1] S. Datta and B. Das, Appl. Phys. Lett. **56**, 665 (1990).

[2] G.A. Prinz, Phys. Today **48**(4), 58 (1995); J.L. Simonds, *ibid.* **48**(4), 26 (1995); E.D. Dahlberg and J.-G. Zhu, *ibid.* **48**(4), 34 (1995); D.D. Awschalom and D.P. Di Vincenzo, *ibid.* **48**(4), 43 (1995); H.J.F. Jansen, *ibid.* **48**(4), 50 (1995).

[3] G. Schmidt, D. Ferrand, L.W. Molenkamp, A.T. Filip, and B.J. van Wees, Phys. Rev. B **62**, R4790 (2000).

[4] R. Fiederling, M. Keim, G. Reuscher, W. Ossau, G. Schmidt, A. Waag, and L.W. Molenkamp, Nature (London) **402**, 787 (1999).

[5] W.C. Black, Jr. and B. Das, J. Appl. Phys. **87**, 6674 (2000).

[6] D.J. Monsma, R. Vlutters, and J.C. Lodder, Science **281**, 407 (1998).

[7] P.S. Anil Kumar and J.C. Lodder, J. Phys. D **33**, 2911 (2000).

[8] R. Cao, K. Miyano, I. Lindau, and W.E. Spicer, J. Electron Spectrosc. Relat. Phenom. **51**, 581 (1990).

[9] C.D. MacPherson, R.A. Wolkow, C.E.J. Mitchell, and A.B. McLean, Phys. Rev. Lett. **77**, 691 (1996).

[10] Q. Guo, M.E. Pemble, and E.M. Williams, Surf. Sci. **468**, 92 (2000).

[11] N. Newman, T. Kendelewicz, L. Bowman, and W.E. Spicer, Appl. Phys. Lett. **46**, 1176 (1985).

[12] T. Kendelewicz, N. Newman, R.S. List, I. Lindau, and W.E. Spicer, J. Vac. Sci. Technol. B **3**, 1206 (1985).

[13] R.S. List, T. Kendelewicz, M.D. Williams, I. Lindau, and W.E. Spicer, J. Vac. Sci. Technol. A **3**, 1002 (1985).

[14] R.H. Williams, A. McKinley, G.J. Hughes, and T.P. Humphreys, J. Vac. Sci. Technol. B **2**, 561 (1984).

[15] L.J. Brillson, and C.F. Brucker, J. Vac. Sci. Technol. **21**, 564 (1982).

[16] G.J. Hughes, P. Ryan, A.A. Cafolla, and P. Quinn, Appl. Surf. Sci. **147**, 201 (1999).

[17] N. Esser, U. Resch-Esser, M. Pristovsek, and W. Richter, Phys. Rev. B **53**, R13 257 (1996).

[18] C. Goletti, N. Esser, U. Resch-Esser, V. Wagner, J. Foeller, M. Pristovsek, and W. Richter, J. Appl. Phys. **81**, 3611 (1997).

[19] T.K. Johal, S.D. Barrett, M. Hopkinson, P. Weightman, and J.R. Power, J. Appl. Phys. **83**, 480 (1998).

[20] W.G. Schmidt, F. Bechstedt, N. Esser, M. Pristovsek, Ch. Schultz, and W. Richter, Phys. Rev. B **57**, 14 596 (1998).

[21] K.B. Ozanyan, P.J. Parbrook, M. Hopkinson, C.R. Whitehouse, Z. Sobiesierski, and D.I. Westwood, J. Appl. Phys. **82**, 474 (1997).

[22] B.X. Yang and H. Hasegawa, Jpn. J. Appl. Phys., Part 1 **33**, 742 (1996).

[23] M.T. Norris, Appl. Phys. Lett. **34**, 282 (1980).

[24] M. Zorn, T. Trepk, J.-T. Zettler, B. Junno, C. Meyne, K. Knorr, T. Wethkamp, M. Klein, M. Miller, W. Richter, and L. Samuelson, Appl. Phys. A: Mater. Sci. Process. **65**, 333 (1997).

[25] L. Li, B.-K. Han, Q. Fu, and R.F. Hicks, Phys. Rev. Lett. **82**, 1879 (1999).

[26] L. Li, B.-K. Han, D. Law, C.H. Li, Q. Fu, and R.F. Hicks, Appl. Phys. Lett. **75**, 683 (1999).

[27] P. Vogt, Th. Hannappel, S. Visbeck, K. Knorr, N. Esser, and W. Richter, Phys. Rev. B **60**, R5117 (1999).

[28] L. Li, Q. Fu, C.H. Li, B.-K. Han, and R.F. Hicks, Phys. Rev. B **61**, 10 223 (2000).

[29] T. Kawamura, Y. Watanabe, Y. Utsumi, K. Uwai, J. Matsui, Y. Kagoshima, Y. Tsusaka, and S. Fujikawa, Appl. Phys. Lett. **77**, 996 (2000).

[30] Th. Hannappel, S. Visbeck, K. Knorr, J. Mahrt, M. Zorn, and F. Willig, Appl. Phys. A: Mater. Sci. Process. **69**, 427 (1999).

[31] J.M. Moison and M. Bensoussan, Surf. Sci. **169**, 68 (1986).

[32] W. Weiss, R. Hornstein, D. Schmeisser, and W. Gpel, J. Vac. Sci. Technol. B **8**, 715 (1990)

[33] J.B. Malherbe and W.O. Barnard, Surf. Sci. **255**, 309 (1991).

[34] M.M. Sung, C. Kim, H. Bu, D.S. Karpuzov, and J.W. Rabalais, Surf. Sci. **322**, 116 (1995).

[35] T. Hashizume, Q.-K. Xue, A. Ichimiya, and T. Sakurai, Phys. Rev. B **51**, 4200 (1995).

[36] P.M. Thibado, E. Kneedler, B.T. Jonker, B.R. Bennett, B.V. Shanabrook, and L.J. Whitman, Phys. Rev. B **53**, R10 481 (1996).

[37] G.W. Anderson, M.C. Hanf, X.R. Qin, P.R. Norton, K. Myrtle, and B. Heinrich, Surf. Sci. **346**, 145 (1996); M. Gester, C. Daboo, S.J. Gray, and J.A.C. Bland, J. Magn. Magn. Mater. **165**, 242 (1997).

[38] M. Gester, C. Daboo, R.J. Hicken, S.J. Gray, A. Ercole, and J.A.C. Bland, J. Appl. Phys. **80**, 347 (1996).

[39] See, for instance, S. Chikazumi, in *Physics of Ferromagnetism* (Clarendon Press, Oxford, 1997); W. J. M. de Jonge, P. J. H. Bloemen, and F. J. A. Broeder, in *Ultrathin Magnetic Structures I*, edited by J. A. C. Bland, and B. Heinrich (Springer-Verlag, Berlin, 1994) p. 65.

[40] W. Wulfhekel, S. Knappmann, and H.P. Oepen, J. Appl. Phys. **79**, 988 (1996).

[41] W.L. O'Brien, T. Droubay, and B.P. Tonner, Phys. Rev. B **54**, 9297 (1996).

[42] A.J.P. Meyer and M.C. Cadeville, J. Appl. Phys. **17** (Suppl. B-I), 223 (1962); K. Huller, G. Dietz, R. Hausmann, and K. Kolpin, J. Magn. Magn. Mater. **53**, 103 (1985).

[43] S. Tanuma, C.J. Powell, and D.R. Penn, Surf. Interface Anal. **17**, 911 (1991).

[44] C.M. Kwei, Y.F. Chen, C.J. Tung, and J.P. Wang, Surf. Sci. **293**, 202 (1993).

[45] W.H. Gries, Surf. Interface Anal. **24**, 38 (1996).